Physics and Imaging in Radiation Oncology 29 (2024) 100545

Contents lists available at ScienceDirect

Physics and Imaging in Radiation Oncology

journal homepage: www.sciencedirect.com/journal/physics-and-imaging-in-radiation-oncology

Original Research Article

Virtual unenhanced dual-energy computed tomography for photon radiotherapy: The effect on dose distribution and cone-beam computed tomography based position verification

Maryam Afifah [a,*], Marloes C. Bulthuis [b], Karin N. Goudschaal [b], Jolanda M. Verbeek-Spijkerman [b], Tezontl S. Rosario [a], Duncan den Boer [a], Karel A. Hinnen [b], Arjan Bel [b], Zdenko van Kesteren [b]

[a] Amsterdam UMC, Location Vrije Universiteit, Department of Radiation Oncology, De Boelelaan 1118, Amsterdam, the Netherlands
[b] Amsterdam UMC, Location University of Amsterdam, Department of Radiation Oncology, Meibergdreef 9, Amsterdam, the Netherlands

ARTICLE INFO

Keywords:
Photon therapy
Dual-energy CT
Virtual unenhanced
Virtual non-contrast
Contrast-enhanced CT
Gynecological irradiation

ABSTRACT

Background and Purpose: Virtual Unenhanced images (VUE) from contrast-enhanced dual-energy computed tomography (DECT) eliminate manual suppression of contrast-enhanced structures (CES) or pre-contrast scans. CT intensity decreases in high-density structures outside the CES following VUE algorithm application. This study assesses VUE's impact on the radiotherapy workflow of gynecological tumors, comparing dose distribution and cone-beam CT-based (CBCT) position verification to contrast-enhanced CT (CECT) images.

Materials and Methods: A total of 14 gynecological patients with contrast-enhanced CT simulation were included. Two CT images were reconstructed: CECT and VUE. Volumetric Modulated Arc Therapy (VMAT) plans generated on CECT were recalculated on VUE using both the CECT lookup table (LUT) and a dedicated VUE LUT. Gamma analysis assessed 3D dose distributions. CECT and VUE images were retrospectively registered to daily CBCT using Chamfer matching algorithm..

Results: Planning target volume (PTV) dose agreement with CECT was within 0.35% for $D_{2\%}$, D_{mean}, and $D_{98\%}$. Organs at risk (OARs) $D_{2\%}$ agreed within 0.36%. A dedicated VUE LUT lead to smaller dose differences, achieving a 100% gamma pass rate for all subjects. VUE imaging showed similar translations and rotations to CECT, with significant but minor translation differences (<0.02 cm). VUE-based registration outperformed CECT. In 24% of CBCT-CECT registrations, inadequate registration was observed due to contrast-related issues, while corresponding VUE images achieved clinically acceptable registrations.

Conclusions: VUE imaging in the radiotherapy workflow is feasible, showing comparable dose distributions and improved CBCT registration results compared to CECT. VUE enables automated bone registration, limiting inter-observer variation in the Image-Guided Radiation Therapy (IGRT) process.

1. Introduction

In abdominal and pelvic tumor radiotherapy (RT) planning, administering an iodine-based contrast agent prior to computed tomography (CT) improves target and organs at risk (OARs) delineation [1–3]. Contrast material is excreted through urination or bowel movements and during RT delivery, no contrast agent is present in the patient. To account for this, delineation and density override of the high-density contrast-enhanced structures (CES) [4] is performed, which directly adds to the clinical workload. Alternatively, an additional pre-contrast CT scan before contrast-enhanced CT (CECT) can be used, introducing uncertainties into the treatment planning workflow due to image registration [5–7] and increasing patient radiation exposure.

Dual-energy CT (DECT) has emerged as a significant advancement in the field of CT [8], allowing material differentiation and decomposition through electron density (ρ_e) and effective atomic number (Z_{eff}) determination. DECT's potential benefits in RT include improved low-energy brachytherapy dose calculations [9,10] and proton stopping power ratio estimation [11–13], where accurate quantification of ρ_e and Z_{eff} is advantageous. However, its advantages are limited in high-energy photon

* Corresponding author at: Amsterdam UMC, locatie VUmc, De Boelelaan 1117, 1081 HV Amsterdam.
E-mail address: m.afifah@amsterdamumc.nl (M. Afifah).

https://doi.org/10.1016/j.phro.2024.100545
Received 7 September 2023; Received in revised form 24 January 2024; Accepted 29 January 2024
Available online 2 February 2024

dose calculations, mainly due to the predominance of Compton scattering, influenced solely by electron density [14]. Nonetheless, additional post-reconstructed DECT images, such as Virtual Monochromatic Images (VMI) for enhanced delineation [15], and the ability to eliminate contrast agent in images, known as 'virtual unenhanced' (VUE) or 'virtual non-contrast' (VNC) imaging [16], show promising applications. The VUE algorithm, using multi-material decomposition (MMD), replaces the estimated volume fraction of contrast agent in each voxel with the same volume fraction of blood, producing iodine-suppressed images [17]. Employing VUE would eliminate the need for additional pre-contrast scans or manual suppression of CES.

Applying the VUE algorithm on datasets containing tissue with substantial calcium content results in a CT number of bony tissue that is significantly lower than that measured in true non-contrast (TNC) images [18–21]. This effect, known as the calcium subtraction artifact [18,20], is crucial in the RT workflow, given the planning CT's key role in radiation therapy. Dose calculation relies on the attenuation of x-rays, determined by electron density derived from the CT number. Additionally, during CBCT-based position verification prior to irradiation, the registration of the CBCT with the planning CT is often based on the visualization of bony anatomy. Therefore, proper understanding of this artifact is essential for accurate dose calculation and patient positioning.

Previous studies on the VUE method have primarily focused on image quality [22], agreement between true non-contrast (TNC) and VUE CT numbers [23,24] and diagnostic applications such as detection of hepatic metastasis [25], urinary stones [26] and gallstones [27]. However, the impact of the calcium subtraction artifact on position verification based on bony anatomy and its effects on dose calculation for pelvic sites receiving contrast agent have not been investigated. Our study aims to assess the feasibility of incorporating VUE images from rapid kVp-switching DECT acquisitions into the RT workflow for gynecological tumors. Our objective is to evaluate the effects of VUE images on dose distribution and position verification compared to CECT images, with the aim of improving our understanding of the applicability of VUE images in gynecological tumor RT.

2. Materials and methods

2.1. Patient population

Fourteen gynecological cancer patients (12 cases of cervical cancer, 2 cases of endometrial cancer, tumor stages IA to IVA, age range 36 to 84 years, 55 years median age) treated between February 2021 and November 2022 were retrospectively included in this study. Informed consent was obtained from all patients prior to their inclusion in the study. Treatment delivery was performed on Elekta Synergy linear accelerator (Elekta Oncology Systems, Crawley, UK) equipped with CBCT, based on a Volumetric Modulated Arc Therapy (VMAT) plan. The prescribed dose was delivered over 25 fractions with a dose of 1.8 Gy per fraction, following a daily online image guided RT (IGRT) protocol. The target volumes consisted of the clinical target volume (CTV) and elective lymph nodes, with a 5 mm margin for the planning treatment volume (PTV).

2.2. CT technique and protocol

All patients were scanned with a single-source rapid kilovolt peak (kVp) switching CT scanner (Revolution CT; General Electric Healthcare, Milwaukee, Wisconsin, USA). The scanner's DECT mode involved rapid switching between high-energy (140 kVp) and low-energy (80 kVp) spectra. The scanning parameters included 128 x 0.625 mm collimation width, automated tube current modulation, 0.8 s revolution time, and 0.992 spiral pitch factor. Following our clinical protocol, DECT datasets of gynecological patients were acquired with the prior administration of three types of iodinated contrast agents; intravenous (IV), vaginal, and small bowel contrast. Approximately 30 to 60 min prior to CT acquisition, small bowel contrast was taken orally (12.5 mL Telebrix Gastro, Meglumine ioxitalamate 660 mg/mL equivalent to 300 mg I/mL) supplemented with water to 1L). Just prior to CT acquisition, vaginal contrast (3 mL Telebrix Gastro diluted with 30 mL ultrasound gel) was slowly administered using a catheter. The IV contrast (90 mL Optiray 350, Ioversol 741 mg/mL equivalent to 350 mg I/mL) was injected intravenously, with a 60 s delay. From the DECT dataset, two reconstructions were generated: a 120 kVp-like CECT reconstruction (approximating conventional single-energy CT 120 kVp images) and a VUE reconstruction, both at 2.5 mm slice thickness. Fig. 1 provides an example of these reconstructions. In the clinical workflow, the 120 kVp-like CECT reconstruction was used. CT numbers of CES and bony anatomy were measured on both CECT and VUE reconstructions for further analysis.

2.3. Treatment planning

A VMAT plan for clinical use was generated in RayStation 9A (RaySearch Laboratories, Stockholm, Sweden) on the CECT. Following our clinical protocol, the CES were semi-automatically delineated using a region growing tool within Raystation based on gray-level thresholding. To avoid underestimation of dose-volume metrics [28–30] a density override (1.00 g/cm^3) was applied on the CES for dose optimization and calculation. The dose was calculated with the Collapsed Cone dose engine (v5.1, dose-to-water) with a $0.2 \times 0.2 \times 0.2$ cm^3 dose grid. The VMAT plan, generated on the CECT, underwent two recalculations on the VUE reconstruction (without a density override) employing identical dose calculation engine and dose grid settings. The first recalculation utilized the CECT lookup table (LUT), while the second recalculation employed a dedicated LUT for VUE images. The following dose-volume histogram (DVH) parameters were extracted: the near minimum ($D_{98\%}$), mean (D_{mean}), and near maximum ($D_{2\%}$) dose of the PTV and near maximum of organs at risk (OARs) such as bladder, rectum, sigmoid, and bowel bag area. DVH parameters based on the VUE images were compared to the DVH parameters based on the CECT (with density override) using a two-tailed Wilcoxon signed-rank test (Statistics and Machine Learning Toolbox, MATLAB 2022b), considering a p-value < 0.05 as statistically significant. Agreement between the dose distribution of CECT (with density override) and both VUE (without density override) dose distributions was evaluated through a gamma analysis (1 %/1mm local gamma, 30% cut-off global maximum dose).

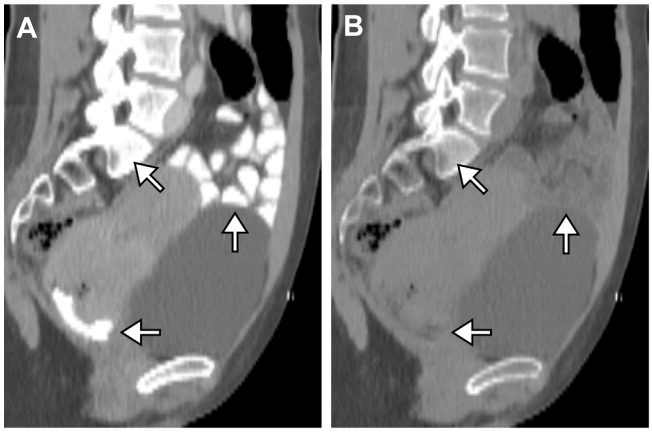

Fig. 1. A) 120 kVp-like reconstruction (sagittal view) from DECT data set. B) Corresponding VUE reconstruction (sagittal view) from the same DECT data set. In the VUE image iodinated contrast agent has been filtered out, while at the same time a CT number reduction in bony material is observed. Both images are displayed at window width (WW) 520 and window level (WL) 20.

2.4. Position verification

Daily CBCT position verification was performed prior to treatment delivery using the XVI system (R5.0.4, Elekta Oncology Systems, Crawley, UK). The protocol for position verification was as follows: a region of interest (ROI) containing the os pubis and os sacrum was used for registration, excluding moving structures (e.g. trochanter minor) from the clipbox. Automatic registration was performed with the 'Bone (T + R)' Chamfer matching algorithm. Registration comprises of segmentation of the corresponding bone regions using thresholds, simplifying them into a binary image to indicate edges of the segmented regions. An optimization based on the Chamfer algorithm [31] minimizes the surface distance between the segmented volumes, resulting in a set of translations in LR, CC and AP-direction and rotations around the LR, CC and AP-axis for the CBCT. The radiotherapy technologist (RTT) visually assessed the agreement of the bone areas and made adjustments to registrations if needed. Inclusion of 14 patients with 25 fractions each resulted in a total of 350 CBCT registrations. During our clinical practice, there were several instances where deviations from this IGRT protocol occurred. These deviations involved switching to another registration algorithm, 'Grey Value (T + R)', on multiple occasions. Additionally, manual adjustments to the registration based on the 'Bone (T + R)' algorithm were performed several times. To obtain a ground truth for proper comparison, the CBCT was retrospectively re-registered to the CECT only using the 'Bone (T + R)' mode within the XVI software. The CBCT was also registered to the corresponding VUE image of the CECT only using the 'Bone (T + R)' mode. Translations and rotations from the VUE image registrations were compared to those from the retrospective CECT image registrations using a two-tailed Wilcoxon signed rank test to test for significant differences.

3. Results

On average, the CT numbers of the CES and bony anatomy were lower on the VUE image compared to CECT. When comparing VUE to CECT images, there was an average reduction of 310 ± 79 HU (337 ± 77 vs. 27 ± 9 HU, $p = 0.018$) in the CT numbers of vaginal contrast structures. Similarly, the CT numbers of small bowel contrast structures showed an average reduction of 175 ± 50 HU (198 ± 50 vs. 24 ± 6 HU, $p < 0.001$) in VUE compared to CECT images. The VUE image also exhibited a reduction in CT numbers for bony tissue, including bone marrow and cortical bone. The delineated bony anatomy showed an average reduction of 114 ± 12 HU (409 ± 38 vs. 295 ± 42 HU, $p < 0.001$) in VUE images compared to CECT.

3.1. Dose distribution

Fig. 2 presents a representative example comparing dose distributions recalculated on the VUE image and the CECT image. Note that the difference map for both LUT's employed focuses on isodose lines that represent less than 1% of the total prescribed dose of 45 Gy to the PTV. For the VUE image, based on the CECT LUT, PTV $D_{2\%}$, D_{mean}, and $D_{98\%}$ parameters differed by a maximum of +0.35% compared to CECT ($p < 0.001$). The mean value of near maximum doses in the OARs (bladder, bowel bag, rectum and sigmoid) differed by a maximum of +0.36% ($p < 0.001$). PTV DVH parameters on the VUE image, employing the dedicated VUE LUT, differed by a maximum of −0.13% compared to CECT ($p < 0.006$), and the mean value of near maximum doses in the OARs differed by a maximum of −0.13% ($p < 0.036$). Table 1 summarizes the results for the 14 subjects. For dose distributions on VUE based on the CECT LUT, in twelve subjects the gamma pass-rate was 100%, the remaining two subjects had a gamma pass rate of 98.1% and 99.7%. The average value of the gamma index (γ_{mean}) was calculated as 0.16 ± 0.03. For VUE based on the dedicated VUE LUT, a gamma pass rate of 100%

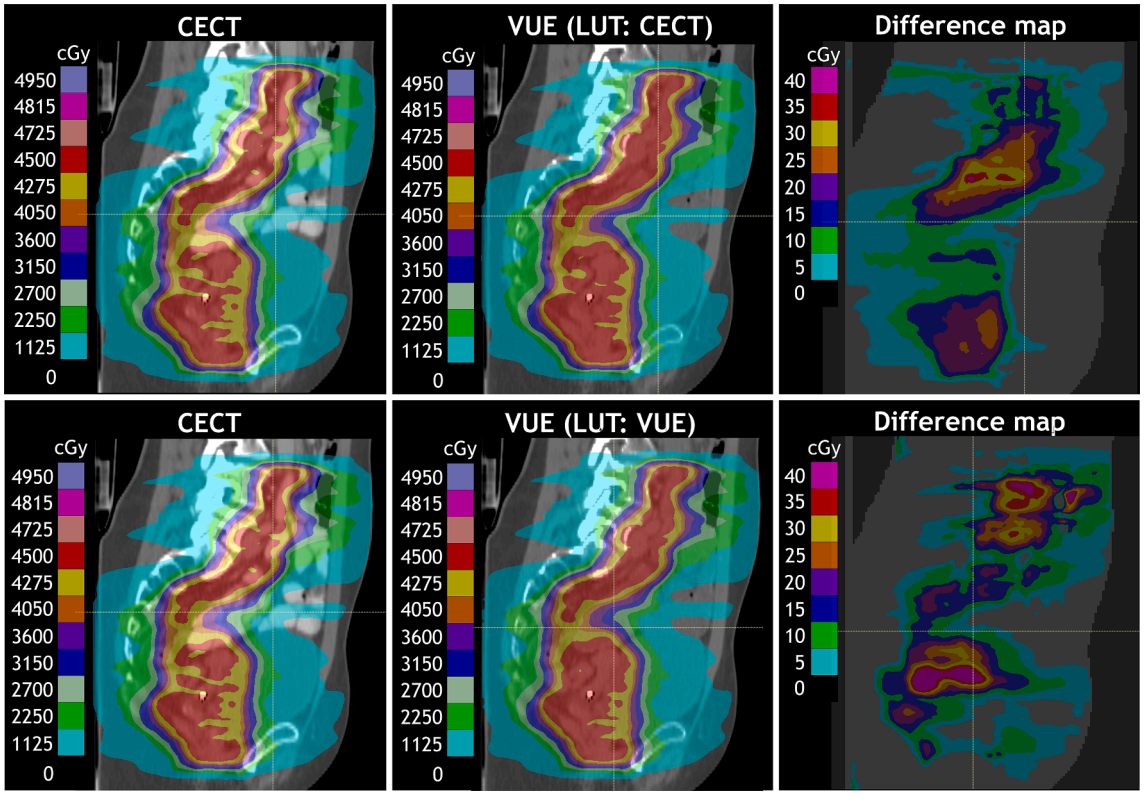

Fig. 2. The dose distribution on the CECT (with density override) and VUE images (on both CECT and dedicated VUE LUT) of a representative patient, along with the corresponding dose difference map.

Table 1
DVH parameters for the treatment target (PTV) and organs at risk (OARs) over the 14 patients receiving 45 Gy to the PTV. Results are shown in Gy.

		CECT (LUT: CECT) Mean [min. – max.]	VUE (LUT: CECT) Mean [min. – max.]	VUE (LUT: VUE) Mean [min. – max.]
PTV	$D_{2\%}$	48.08 [46.15 – 56.32]	48.25 [46.35 – 56.53]	48.03 [46.14 – 56.20]
	D_{mean}	45.16 [44.92 – 45.60]	45.32 [45.09 – 45.78]	45.12 [44.87 – 45.52]
	$D_{98\%}$	41.88 [41.56 – 42.01]	42.00 [41.69 – 42.14]	41.84 [41.52 – 41.99]
Bladder	$D_{2\%}$	45.84 [45.31 – 46.22]	46.00 [45.49 – 46.34]	45.78 [45.23 – 46.15]
Bowel bag	$D_{2\%}$	44.83 [41.52 – 46.23]	44.99 [41.65 – 46.33]	44.81 [41.51 – 46.16]
Rectum	$D_{2\%}$	45.64 [44.93 – 46.08]	45.81 [45.13 – 46.24]	45.59 [44.80 – 45.95]
Sigmoid	$D_{2\%}$	45.82 [45.05 – 46.42]	45.98 [45.17 – 46.53]	45.77 [44.99 – 46.40]

was achieved for all 14 subjects. The average value of the gamma index (γ_{mean}) was 0.07 ± 0.02.

3.2. Position verification

Out of 350 CBCT images re-registered to the CECT only using the 'Bone (T + R)' Chamfer matching algorithm, 85 cases (distributed across 8 patients) showed inadequate registration quality upon visual assessment. This was primarily due to misaligned bony anatomy, as illustrated in Fig. 3 (upper panels). For one patient, none of the 25 registrations were of adequate quality (subject 10). In contrast, CBCT registrations using the same algorithm to the corresponding VUE image had no reported poor quality registrations. Consequently, only the CBCT registrations demonstrating proper alignment with both the CECT and VUE images were included in the subsequent analysis. This selection ensures comparisons between valid, and thus clinically applicable, registrations.

As an example, Fig. 4 showcases the translations in AP direction and rotations around the AP-axis for each patient and the overall patient population; LR and CC distributions yielded similar results. Table 2 summarizes registration results for all directions and rotation axes. The rotations around each axis in the CBCT registrations, when registered to the VUE reconstruction, did not significantly differ from the registrations based on the CECT reference sets. Statistically significant differences were observed in the translation distributions. However, the mean values varied by a maximum of 0.02 cm, with median translation difference values of 0.01 cm for LR, CC and AP-direction. Median rotation differences were 0.0° around all three axes.

4. Discussion

In our study, we compared the RT workflow using VUE imaging to the standard workflow with contrast-enhanced CT as planning and reference CT. We found good dosimetrical agreement between the clinical VMAT plans on CECT and recalculated plans on VUE images. VUE imaging in our IGRT workflow showed comparable translations and rotations to CECT-based IGRT. Based on these findings, VUE imaging proved superior in the RT workflow compared to our current clinical practice.

Using VUE images in treatment planning has several benefits, depending on the adopted CES accounting strategy. Orally administered contrast agents generally reduces radiation doses to the target volume and OARs in treatment planning compared to non-contrasted plans [28–30]. VUE eliminates manual CES delineation and density overrides, streamlining treatment planning workflow.

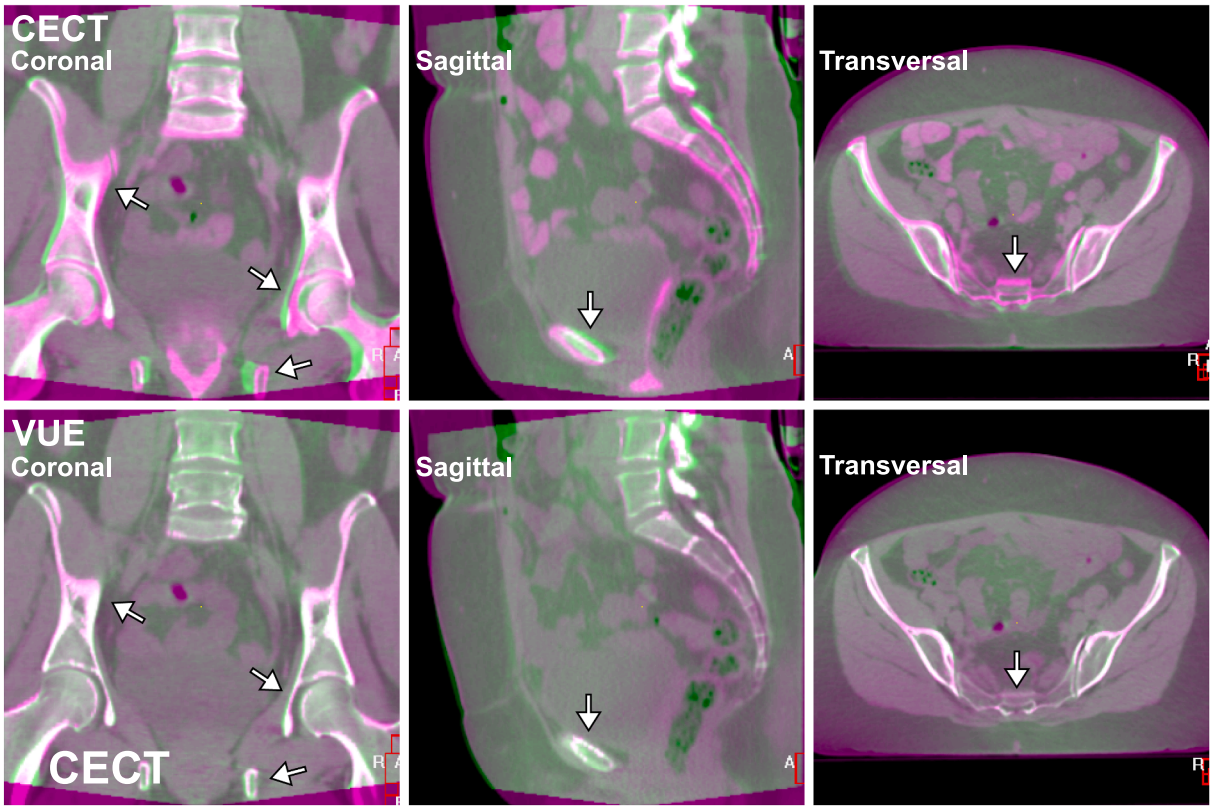

Fig. 3. Example of automatic registration using the 'Bone (T + R)' algorithm to the CECT resulting in an inadequate registration and automatic registration using the 'Bone (T + R)' algorithm of the same CBCT to the corresponding VUE image. Reference CT is displayed in purple and CBCT in green. (For interpretation of the references to colour in this figure legend, the reader is referred to the web version of this article.)

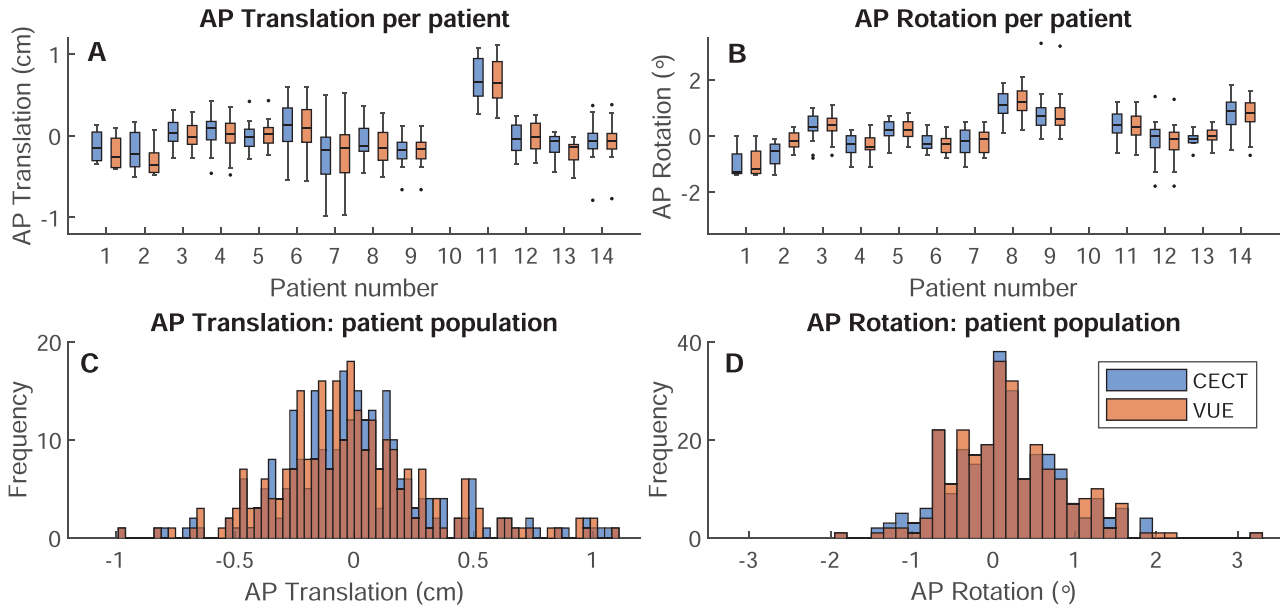

Fig. 4. A & B) AP translations of the registrations of CBCT to CECT (blue) and VUE (red) per patient. Boxplots show the inter-quartile range (IQR). Whiskers indicate the outermost points within 1.5 × IQR and the points beyond that are outliers. Notably, for subject 10, the registration to CECT yielded zero clinically acceptable registrations. C & D) Registration of CBCT to CECT (blue) and VUE (red) in AP direction over the patient population. (For interpretation of the references to colour in this figure legend, the reader is referred to the web version of this article.)

Table 2
Mean values of distributions over the patient population in translation in LR, CC and AP-direction and rotations around the LR, CC and AP-axis. Reported *p*-values are obtained from a two-tailed Wilcoxon signed rank test.

	LR (cm)		CC (cm)		AP (cm)		LR-axis(°)		CC-axis(°)		AP-axis(°)	
	CECT	VUE	CECT	VUE	CECT	VUE	CECT	VUE	CECT	VUE	CECT	VUE
Population mean	−0.01	0.00	0.04	0.02	0.00	−0.02	0.39	0.42	0.07	0.12	0.15	0.18
SD	0.37	0.37	0.29	0.29	0.33	0.33	1.74	1.73	0.90	0.87	0.70	0.67
p-value	<0.001		<0.001		<0.001		0.670		0.261		0.170	

Another common strategy to account for the CES involves consecutive CT scanning with pre-contrast (TNC) and post-contrast (CE) acquisitions [3,5], requiring subsequent image registration using rigid or deformable image registration (DIR). This approach introduces image registration uncertainties and the possibility of geometric misalignment between the acquisitions, with errors in pelvic sites ranging up to 6 mm [7]. By using VUE, the additional pre-contrast CT scan can be omitted, reducing patient imaging dose and eliminating uncertainties in registration.

Several studies explored the dosimetric equivalence of VUE imaging and pre-contrast CT in treatment planning. Noid et al. found minimal differences (0.2%, 0.1%, and 0.1%) in PTV DVH parameters between non-contrast and VUE IMRT plans for pancreatic patients [5]. Koike et al. observed maximum variations of 0.23% in PTV DVH parameters and 1.4% in mandible D_{max} for head and neck plans [19]. On the other hand, Ohira et al. observed a D_{max} error of 0.6% for the mandible in nasopharyngeal plans using separate lookup tables (LUT) for pre-contrast and post-contrast data sets [32]. Edmund et al. found differences within 2% between VUE and pre-contrast CT, which they attribute to anatomical changes [15]. All studies used a pre-contrast scan for dose calculation and a post-contrast scan for delineation. To correct misalignment between the pre- and post-contrast images, VUE images were fused with the pre-contrast images using a DIR or rigid registration. In our workflow, we did not use a pre-contrast scan, eliminating additional uncertainties associated with registration.

The reduction in CT numbers in regions without iodinated contrast agent with VUE imaging can be attributed to the absence of calcium as a base material in the two- or three-material decomposition algorithms for generating VUE images, resulting in false subtraction [33]. However, the decrease in CT numbers during gynecological tumor treatment planning had minimal dosimetric impact. Applying a specific LUT for VUE images further reduced the dose difference. Nevertheless, using a single LUT for both CECT and VUE images would not lead to clinically significant differences in practical applications. We focused on gynecological VMAT plans and applied a density override on the CES. Similar dosimetric errors can be expected for other pelvic targets such as prostate, bladder, and rectal cancers.

One limitation of our study is the reporting of doses as dose-to-water (D_w). While this approach considers variations in tissue densities, attenuation, and scatter factors, it presents the dose at each location as D_w. An analysis using dose-to-medium (D_m) would highlight dosimetric differences in the high-density regions (bone). Nevertheless, since the volume of cortical bone within our study's target volumes is relatively small, conducting an analysis based on D_m would have minimal impact. To assess uncertainty in semi-automatic CES delineation on CECT, we recalculated distributions for the 5 subjects with the largest CES volumes. This involved a 2 mm uniform expansion and contraction to the CES with a 1.00 g/cm^3 density override. Recalculated dose distributions showed a maximum 0.05 Gy (0.1%) difference to the PTV, relative to the prescribed 45 Gy dose. Delineation uncertainty minimally affects the CECT reference distribution.

This study is the first to demonstrate that VUE images can be safely used for position verification in a bony anatomy-based IGRT workflow, despite the observed density reduction effect in the bony anatomy. Automated bone registration using the Chamfer match algorithm for the CBCT to the VUE image as reference CT yielded translations and

rotations comparable to those obtained from CBCT registration to the CECT image. The differences in translation and rotation between CECT and VUE were found to be within the range of tenths of millimeters and degrees, respectively. These differences in magnitude are considered clinically irrelevant within the context of the IGRT workflow.

Moreover, in 24% of the registrations, the CECT presumably suffered from contrast, while the VUE images did not. The CES on the CECT then caused an incorrect segmentation of high-density structures used for the registration, while on the CBCT no corresponding contrast areas were present, resulting in an erroneous minimized distance between segmented bone areas. Therefore, VUE imaging enables a robust and automated bone registration regimen which is not possible for CECT, effectively reducing inter-observer variation in the IGRT process.

Our study successfully incorporated VUE into the RT workflow for treatment planning and bone registration in the IGRT process. DECT can be performed without radiation penalty or impaired image quality compared to conventional SECT [34–37]. By using VUE, the need for a pre-contrast scan is eliminated, reducing patient radiation dose by half compared to a SECT consecutive scanning protocol.

While our study focused on implementing VUE generated from the GE Revolution DECT scanner, further investigation is needed to determine if other commercial DECT scanner models offer similar accuracy, precision, and limitations. It is anticipated that similar results can be achieved with other dose calculation algorithms and bone registration software.

In conclusion, VUE imaging in the RT workflow for gynecological tumors is feasible and comparable in accuracy to the current clinical practice that involves contrast-enhanced CT images. Moreover, the presence of contrast agent in contrast-enhanced CT images can affect the accuracy of bone registration, while VUE images do not exhibit this behavior. As a result, the implementation of VUE enables an automated IGRT workflow, thereby reducing inter-observer variation in the registration process.

Ethics approval and consent to participate

The institutional ethics committee (Academic Medical Center, University of Amsterdam, Amsterdam, NL) granted an exemption from requiring ethics approval in this study. Written informed consent was obtained from all subjects prior to study enrollment.

Consent for publication

Figures depicting individual person's data are unidentifiable and there are no details on individuals reported within the manuscript. Therefore, separate consent for publication is not necessary for the figures and results shown in this manuscript.

CRediT authorship contribution statement

Maryam Afifah: Conceptualization, Methodology, Investigation, Formal analysis, Writing – original draft, Writing – review & editing, Visualization, Supervision, Project administration, Funding acquisition. **Marloes C. Bulthuis:** Investigation, Resources, Writing – review & editing. **Karin N. Goudschaal:** Investigation, Resources, Writing – review & editing. **Jolanda M. Verbeek-Spijkerman:** Conceptualization, Writing – review & editing. **Tezontl S. Rosario:** Conceptualization, Methodology, Writing – review & editing. **Duncan den Boer:** Conceptualization, Methodology, Writing – review & editing. **Karel A. Hinnen:** Conceptualization, Methodology, Writing – review & editing. **Arjan Bel:** Methodology, Funding acquisition, Writing – review & editing. **Zdenko van Kesteren:** Conceptualization, Methodology, Formal analysis, Supervision, Funding acquisition, Writing – review & editing.

Declaration of competing interest

The authors declare the following financial interests/personal relationships which may be considered as potential competing interests: Arjan Bel is involved in several collaboration projects with Elekta AB, Stockholm, Sweden and Varian, Palo Alto, USA, outside of this work. Zdenko van Kesteren is collaborating in research of several Varian and Philips Healthcare sponsored projects outside of this work. Arjan Bel, Maryam Afifah and Zdenko van Kesteren have a research collaboration with GE Healthcare. This study was partly funded by GE Healthcare, Milwaukee, Wisconsin, USA. However, GE Healthcareand the other mentioned companies had no involvement in study design, data collection and analysis, or writing of the manuscript. The other authors have no relevant conflicts of interest to disclose.

References

[1] Jabbour S, Hashem S, Bosch W, Kim T, Finkelstein S, Anderson BM, et al. Upper abdominal normal organ contouring guidelines and atlas: A Radiation Therapy Oncology Group consensus. Pract Radiat Oncol 2014;4:82–9.
[2] Gay H, Barthold H, O'Meara E, Bosch WR, El Naqa I, Al-Lozi R, et al. Pelvic normal tissue contouring guidelines for radiation therapy: A radiation therapy oncology group consensus panel atlas. Int J Radiat Oncol Biol Phys 2012;83:353–62.
[3] Small W, Bosch WR, Harkenrider MM, Strauss JB, Abu-Rustum N, Albuquerque KV, et al. NRG oncology/RTOG consensus guidelines for delineation of clinical target volume for intensity modulated pelvic radiation therapy in postoperative treatment of endometrial and cervical cancer: an update. Int J Radiat Oncol Biol Phys 2021;109:413–24.
[4] Feng CH, Hasan Y, Kopec M, Al-Hallaq HA. Simultaneously integrated boost (SIB) spares OAR and reduces treatment time in locally advanced cervical cancer. J Appl Clin Med Phys 2016;17:76–89.
[5] Noid G, Schott D, Paulson E, Zhu J, Shah J, Li XA. Technical Note: Using virtual noncontrast images from dual-energy CT to eliminate the need of precontrast CT for x-ray radiation treatment planning of abdominal tumors. Med Phys 2021;48:1365–71.
[6] Yang D, Chaudhari SR, Goddu SM, Pratt D, Khullar D, Deasy JO, et al. Deformable registration of abdominal kilovoltage treatment planning CT and tomotherapy daily megavoltage CT for treatment adaptation. Med Phys 2009;36:329–38.
[7] Loi G, Fusella M, Lanzi E, Cagni E, Garibaldi C, Iacoviello G, et al. Performance of commercially available deformable image registration platforms for contour propagation using patient-based computational phantoms: A multi-institutional study. Med Phys 2018;45:748–57.
[8] van Elmpt W, Landry G, Das M, Verhaegen F. Dual energy CT in radiotherapy: Current applications and future outlook. Radiother Oncol 2016;119(1).137–144–8.
[9] Landry G, Gaudreault M, van Elmpt W, Wildberger JE, Verhaegen F. Improved dose calculation accuracy for low energy brachytherapy by optimizing dual energy CT imaging protocols for noise reduction using sinogram affirmed iterative reconstruction. Med Phys 2016;26:75–87.
[10] Remy C, Lalonde A, Béliveau-Nadeau D, Carrier JF, Bouchard H. Dosimetric impact of dual-energy CT tissue segmentation for low-energy prostate brachytherapy: A Monte Carlo study. Phys Med Biol 2018;63(2):025013.
[11] Peters N, Wohlfahrt P, Hofmann C, Möhler C, Menkel S, Tschiche M, et al. Reduction of clinical safety margins in proton therapy enabled by the clinical implementation of dual-energy CT for direct stopping-power prediction. Radiother Oncol 2022;166:71–8.
[12] Taasti VT, Decabooter E, Eekers D, Compter I, Rinaldi I, Bogowicz M, et al. Clinical benefit of range uncertainty reduction in proton treatment planning based on dual-energy CT for neuro-oncological patients. Br J Radiol 2023;96:20230110.
[13] Sabouri P, Koroulakis A, Cusatis D, Lehman K, Wohlfahrt P, Shah J, et al. Treatment plan dose comparison for proton therapy using single energy and dual energy computed tomography simulation methods. Int J Radiat Oncol 2023;117:e699.
[14] Binjola A. Interaction of Radiation with Matter. In: Mallick S, Rath G, Benson R, editors. Pract. Radiat. Oncol. Singapore: Springer; 2019. p. 1–300.
[15] Edmund J, Rønjom MF, Overeem Felter M, Maare C, Dam AMJ, Tsaggari EPW. Split-filter dual energy computed tomography radiotherapy: From calibration to image guidance. Phys Imaging Radiat Oncol 2023;28:100495.
[16] Harsaker V, Jensen K, Andersen HK, Martinsen AC. Quantitative benchmarking of iodine imaging for two CT spectral imaging technologies: a phantom study. Eur Radiol Exp 2021;5(1):24.
[17] Slavic S, Danielsson M. Dual-energy: The GE approach. Cham, Switzerland: Springer International Publishing; 2022. p. 45–62.
[18] Popnoe DO, Ng CS, Zhou S, Kaur H, Kang HC, Loyer EM, et al. Comparison of virtual to true unenhanced abdominal computed tomography images acquired using rapid kV-switching dual energy imaging. PLoS One 2020;15(9):e0238582.
[19] Koike Y, Ohira S, Akino Y, Sagawa T, Yagi M, Ueda Y, et al. Deep learning-based virtual noncontrast CT for volumetric modulated arc therapy planning: Comparison with a dual-energy CT-based approach. Med Phys 2020;47:371–9.
[20] Xiao JM, Hippe DS, Zecevic M, Zamora DA, Cai LM, Toia GV, et al. Virtual unenhanced dual-energy CT images obtained with a multimaterial decomposition

algorithm: Diagnostic value for renal mass and urinary stone evaluation. Radiology 2021;298:611–9.
[21] Parakh A, Lennartz S, An C, Rajiah P, Yeh BM, Simeone FJ, et al. Dual-energy CT images: Pearls and pitfalls. Radiographics 2021;41:98–119.
[22] Li Y, Li Y, Jackson A, Li X, Huang N, Guo C, et al. Comparison of virtual unenhanced CT images of the abdomen under different iodine flow rates. Abdom Radiol 2017;42:312–21.
[23] Borhani AA, Kulzer M, Iranpour N, Ghodadra A, Sparrow M, Furlan A, et al. Comparison of true unenhanced and virtual unenhanced (VUE) attenuation values in abdominopelvic single-source rapid kilovoltage-switching spectral CT. Abdom Radiol 2017;42:710–7.
[24] Lacroix M, Mulé S, Herin E, Pigneur F, Richard P, Zegai B, et al. Virtual unenhanced imaging of the liver derived from 160-mm rapid-switching dual-energy CT (rsDECT): Comparison of the accuracy of attenuation values and solid liver lesion conspicuity with native unenhanced images. Eur J Radiol 2020;133:109387.
[25] Tian SF, Liu AL, Liu JH, Sun MY, Wang HQ, Liu YJ. Application of computed tomography virtual noncontrast spectral imaging in evaluation of hepatic metastases: A preliminary study. Chin Med J (Engl) 2015;128:610–4.
[26] Cheng Y, Sun J, Li J, Han Y, Zhang X, Zhang L, et al. The Added Value of Virtual Unenhanced Images Obtained From Dual-energy CT Urography in the Detection and Measurement of Urinary Stone. Urology 2022;166:118–25.
[27] Yang CB, Zhang S, Jia YJ, Duan HF, Ma GM, Zhang XR, et al. Clinical Application of Dual-Energy Spectral Computed Tomography in Detecting Cholesterol Gallstones From Surrounding Bile. Acad Radiol 2017;24:478–82.
[28] Heydarheydari S, Farshchian N, Haghparast A. Influence of the contrast agents on treatment planning dose calculations of prostate and rectal cancers. Reports Pract Oncol Radiother 2016;21:441–6.
[29] Jing H, Tian Y, Tang Y, Wang SL, Jin J, Song YW, et al. Oral contrast agents lead to underestimation of dose calculation in volumetric-modulated arc therapy planning for pelvic irradiation. Chin Med J (Engl) 2020;133:2061–70.
[30] Montero-Oleas N, Imbaquingo-Cabrera A, Coloma-Espin A, Collantes-Cruz V, Molineros C. Dosimetric effects of oral contrast in the planning of conventional radiotherapy and IMRT, for rectal cancer treatment. J Radiother Pract 2023;22:e54.
[31] Borgefors G. Hierarchical Chamfer Matching: A Parametric Edge Matching Algorithm. IEEE Trans Pattern Anal Mach Intell 1988;10:849–65.
[32] Ohira S, Komiyama R, Koike Y, Washio H, Kanayama N, Inui S, et al. Dual-energy computed tomography image-based volumetric-modulated arc therapy planning for reducing the effect of contrast-enhanced agent on dose distributions. Med Dosim 2021;46:328–34.
[33] Mendonca PR, Lamb P, Sahani DV. A flexible method for multi-material decomposition of dual-energy CT images. IEEE Trans Med Imaging 2014;33:99–116.
[34] Clark ZE, Bolus DN, Little MD, Morgan DE. Abdominal rapid-kVp-switching dual-energy MDCT with reduced IV contrast compared to conventional MDCT with standard weight-based IV contrast: an intra-patient comparison. Abdom Imaging 2014;40:852–8.
[35] Wichmann JL, Hardie AD, Schoepf UJ, Felmly LM, Perry JD, Varga-Szemes A, et al. Single- and dual-energy CT of the abdomen: comparison of radiation dose and image quality of 2nd and 3rd generation dual-source CT. Eur Radiol 2017;27:642–50.
[36] Wortman JR, Shyu JY, Dileo J, Uyeda JW, Sodickson AD. Dual-energy CT for routine imaging of the abdomen and pelvis: radiation dose and image quality. Emerg Radiol 2020;27:45–50.
[37] Lenga L, Lange M, Martin SS, Albrecht MH, Booz C, Yel I, et al. Head and neck single-and dual-energy CT: differences in radiation dose and image quality of 2nd and 3rd generation dual-source CT Br. J Radiol 2021;94(1122). 20210069.